TÜBİTAK

Turkish Journal of Engineering & Environmental Sciences

http://journals.tubitak.gov.tr/engineering/

Research Article

Turkish J Eng Env Sci
(2014) 38: 323 – 337

doi:10.3906/muh-1304-9

The influence of overburden pressure on liquefaction potential

Gholam MORADI, Mehdi Hosseinzadeh SOTOUBADI, Behnam Rahrou KHATIBI*
Department of Civil Engineering, University of Tabriz, Tabriz, Iran

Received: 14.04.2013 • **Accepted/Published Online:** 10.04.2015 • **Printed:** 04.03.2016

Abstract: One of the important design considerations for structures situated on sand deposits is the potential for instability caused by the development of excess pore water pressure as a result of earthquake loading. A build-up of excess pore water pressure may lead to initial liquefaction. In this paper, to examine the influence of overburden pressure on liquefaction potential, equivalent loads of several buildings with various stories were loaded on a sandy soil deposit using the FLAC program. The pore water pressure ratio r_u was defined for the program by a Fish function. Analyses showed that by increasing the applied loading due to building construction, the values of effective stress and shear stress in the soil mass increased, and this generally can be a factor to influence liquefaction potential. Furthermore, dynamic analyses showed that there was a shallow longitudinal area beneath tall buildings in which liquefaction potential increased due to stress concentration and high confining effective stress; generally, they can be named as the factors to increase liquefaction potential.

Key words: Liquefaction potential, overloading, geotechnical engineering, finite difference method, Finn constitutive model

1. Introduction

When saturated sand deposits are subjected to earthquake-induced shaking, pore water pressure in the soil starts to progressively build up, which leads to loss of soil shear strength. Liquefaction is the extreme manifestation of this phenomenon. At the commencement of soil liquefaction, the effective stress in the soil becomes zero and pore water pressure in the soil becomes equal to the initial static effective stress. Major earthquakes occurring during past years, such as the 1964 Niigata and Alaska, 1989 Loma Prieta, and 1999 İzmit events, have demonstrated the damaging effects of soil liquefaction. Thus, it is important to investigate this phenomenon and present suitable methods to avoid such damages.

As mentioned above, most of the time, the liquefaction phenomenon occurs in loose saturated sandy soils situated in regions prone to earthquakes. When a saturated loose sand deposit is subjected to earthquake shaking, because the value of the void ratio (e) is high, applied shear stress on the soil mass leads to reduce the volume of the soil mass, and because the soil mass is saturated, this tendency toward reduction of volume leads to an increase in pore water pressure. In these cases, during dynamic loading there is not enough time to drain the excess pore water and, therefore, pore water pressure in the soil mass starts to progressively build up and effective stress tends toward zero. In such situations, the soil mass shows liquid behavior and does not have enough shear strength. Settlements, sand boiling, lateral spreads, lateral flows, loss of lateral support, loss of bearing support, and floatation of bearing supports are examples of consequences of this phenomenon.

*Correspondence: behnam.rahro@gmail.com

The pore water pressure ratio (r_u) can be employed to examine the liquefaction process, which is usually defined as the ratio of pore water pressure to the initial static mean effective stress in the soil. During cyclic loading in the loose saturated sandy soil, pore water pressure starts to progressively build up, and shear strain of the soil mass progressively increases and parameter r_u tends toward 1.0. In this situation, the soil mass might experience maximum shear strains and deformations because there is not enough shear strength.

Investigation on soil liquefaction is one of the main subjects in recent decades. Some researchers have studied the assessment of liquefaction potential by in situ methods (e.g., Seed and Idriss [1]) and numerical simulations (e.g., Liyanathirana and Poulos [2]). Results of these investigations are helpful for prediction of liquefaction occurrence in lands situated on regions prone to earthquakes. Therefore, it is important to determine effective factors on the liquefaction potential of soil. It seems that most of the studies in this subject are about the nature of soil liquefaction and how it affects the environment. Recently, some researchers have done examinations about the influence of external loading (such as building, embankment, etc.) on liquefaction potential [3–5]. This means that they would like to know how external loading affects the liquefaction potential. Answering this question requires investigation of soil properties affected by external loading. Most of the studies can be classified into two major categories: the influence of overburden pressure on 1) soil properties and 2) liquefaction potential (see Sections 1.1 and 1.2).

Generally, it is tried to determine the influence of overburden on liquefaction potential and to compare pore water pressure distribution between the case loaded by building construction and the case without existence of a building. For this aim, a sand deposit with liquefaction potential was simulated in FLAC using the Finn constitutive model. The Finn model incorporates equations of Martin et al. [6] and Byrne [7] into the standard Mohr–Coulomb plasticity model. Parameter $(N_1)_{60}$ is the main factor for the Byrne formula [7], so in the present study some parameters required for the Mohr–Coulomb plasticity model were defined for the program by equations that relate them to $(N_1)_{60}$. For consideration of overburden on soil behavior and liquefaction potential under cyclic loading conditions, equivalent loads of 5-, 10-, 15-, and 20-story buildings and the combined loads of them were applied to the deposit. Furthermore, as a cyclic loading, acceleration time history of the Bam earthquake was used. That earthquake occurred on 26 December 2003 in the city of Bam, Iran, with magnitude $M_w = 6.6$. Generally, it is tried to simulate the liquefaction phenomenon in FLAC using parameter $(N_1)_{60}$ as a main factor for soil properties required for the software.

1.1. The influence of overburden pressure on soil properties

Rollins and Seed [3] introduced three factors to evaluate the effect of overburden pressure on liquefaction potential. These factors are static shear stress, effective confining pressure, and overconsolidated ratio (OCR). Generally, any action for increase of soil density can lead to reduction of liquefaction potential because when saturated dense sand is induced by cyclic loading, the soil mass tends to dilate. In this state, pore water pressure evolution becomes negative and effective stress becomes more than its initial value, and the shear strength of the soil mass increases.

1.1.1. Static shear stress

Overburden stress and slope situation may induce the anisotropy consolidated condition and initial static shear stress in the soil mass. According to related studies, static shear stress may affect soil liquefaction potential directly. Lee and Seed [8] indicated that the liquefaction resistance of soil is increased by the increasing of the static shear stress. Increase of initial static shear stress in the soil mass may lead to increase of soil settlement

and compression and, subsequently, it leads to the increase of the cyclic resistant ratio (CRR):

$$CRR = \frac{\tau_{cy}}{\acute{\sigma_{v0}}} \tag{1}$$

where τ_{cy} is cyclic shear strength and $\acute{\sigma_v}$ is vertical effective stress.

Yoshimi and Oh-Oka [9] and Yoshimi and Tokimatsu [4] showed findings in contrast to the above results. According to their results, the CRR may decrease or stay constant as initial static shear stress increases. Thus, the isotropic consolidated state of laboratory testing might be unreliable.

1.1.2. Confining pressure

Using the results of dynamic triaxial testing, Peacock and Seed [10] indicated that cyclic shear stress increases as effective confining pressure increases, but the CRR is contrary. Mulilis et al. [11] denoted that the CRR may slightly decrease with increase of effective confining pressure. This is true for soil specimens prepared by any method. Hynes and Olsen [12] indicated that CRR values decrease by increasing confining effective stress. They concluded that several factors such as method of deposition, stress history, aging effects, and density may affect the influence of confining stress variation on the CRR.

1.1.3. Overconsolidation ratio

According to related studies, the overconsolidation state is an important effect for soil liquefaction potential. If a soil mass has experienced stresses higher than its current state, it is an overconsolidated soil (OCR $>$ 1). Overconsolidated soils have fewer settlements due to external loadings as compared with normally consolidated soils. Seed and Idriss [1] showed that the liquefaction resistance increases as the OCR increases. By using cyclic torsion shear test, Ishihara and Takatsu [13] evaluated the relations between OCR, K_0, and cyclic shear strength. As shown in their results, under constant K_0, the cyclic stress ratio increases by increase of the OCR value.

1.2. The effect of building constructions on liquefaction potential

Liu and Qiao [5], Yoshimi and Tokimatsu [4], and Whitman and Lambe [14] studied the effect of soil liquefaction potential induced by buildings with different laboratory facilities. Yoshimi and Tokimatsu [4] showed that soil liquefaction strength decreased significantly beneath the building by shaking table tests. Whitman and Lambe [14] also concluded similar results by centrifuge model tests.

Existing buildings or any structures affect soil properties such as relative density (D_r), static shear stress, confining pressure, and OCR. It seems that by getting away from the structure's soil foundation, the effect of the existing building or any structure on soil properties becomes negligible, but Lopez and Modaressi [15] indicated that the pore water pressure distribution at the end of the earthquake motion is modified by the presence of the structure, even if the soil profile is far from it.

The potential for liquefaction in soil near a building is generally determined by treating the soil as if it were in the free field under level-ground conditions. However, a review of field case histories, model test results, and a limited number of numerical analyses indicates that the potential for pore water pressure generation near a building may be substantially different from the free field. So far, a number of building types on sands at various relative densities have been analyzed. The analyses were patterned after the Seed–Lee–Idriss procedure, frequently used in liquefaction analyses for dams. Consideration was also given to bearing

capacity failure, settlement, and pore water pressure redistribution following earthquake shaking. Based on the results of numerical and laboratory studies, it is difficult to find case histories where the buildings increased the liquefaction potential compared to free field areas.

2. Definition of the soil profile and its properties

In this study, the soil profile consists of two types: the first type was assumed to be saturated loose sand 30 m in height and the second type assumed to be dry and relatively dense sand of 2 m in height that overlies the loose sand, so the water level is at depth of 2 m from the surface. Defining the dense upper layer helps the model to be close to reality because, in the field, it is relatively impossible to build any structure on fully saturated soil (N.W.T. equals zero from the surface). Furthermore, the length of soil mass was assumed to be 400 m (how this length was selected is described next). It was supposed that during static loading (by applying the equivalent load of buildings), pore water can drain and excess pore water pressure can be released due to external loading. When applying earthquake loading, since it occurs suddenly, there is not enough time to drain pore water and release pore water pressure, and it was supposed that there is no water flow in the soil mass model.

According to Figure 1, the grid size in the middle region of this mesh was selected as small enough to satisfy the required level of precision and the equivalent load of the building was imposed on this area to examine the effect of it on liquefaction potential of the soil deposit. Width of loaded area was assumed as 30 m and length of the third dimension of the model was assumed as 1 m, because the used version of FLAC is 2D.

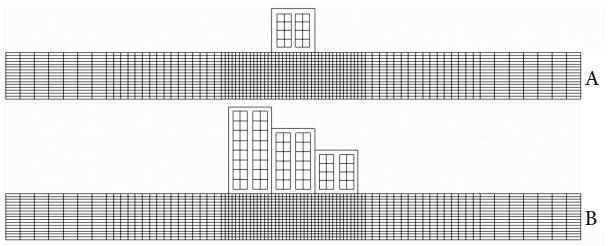

Figure 1. Physical schema of the soil mass mesh and location of loaded area: **A)** one building, **B)** three neighboring buildings (horizontal and vertical scales are different).

3. An introduction to the software and modeling procedure

For modeling the soil mass with liquefaction potential, FLAC software was used. The finite difference method for analysis of soil mass was used in FLAC. The Finn constitutive model is considered as the default in FLAC that facilitates the ability of soil modeling in liquefaction states. In this research, the equivalent linear method and the Finn constitutive method were used.

With FLAC, the effects of pore water pressure with or without loss of pore water pressure can be obtained. The generation of pore water pressure can also be calculated by considering the irrecoverable volumetric strain on the basic Finn model with the dynamic option. In this model, it is assumed that the void ratio is constant; also, it can be calculated as a function of volumetric strain and other parameters can be defined by the void ratio [16].

3.1. Finn constitutive model

Although it seems that pore pressure generation is a primary effect of a cyclic loading, Martin et al. [6] stated that the irrecoverable volume contraction is a primary effect of a cyclic loading. Thus, they supplied the following

empirical equation that relates the increment of volume decrease, $\Delta\epsilon_{vd}$, to the cyclic shear-strain amplitude, γ, where γ is presumed to be the "engineering" shear strain:

$$\Delta\epsilon_{vd} = C_1\left(\gamma - C_2\epsilon_{vd}\right) + \frac{C_3\epsilon_{vd}^2}{\gamma + C_4\epsilon_{vd}} \tag{2}$$

where C_1, C_2, C_3, and C_4 are constants that are related as follows: $C_1C_2C_4 = C_3$.

Subsequently, Byrne [7] proposed a modified and simpler volume change model with two calibration parameters:

$$\frac{\Delta\epsilon_{vd}}{\gamma} = C_1 \exp\left(-C_2\left(\frac{\epsilon_{vd}}{\gamma}\right)\right) \tag{3}$$

where C_1 and C_2 are constants with different definitions from those of Eq. (2). In many cases, $C_2 = 0.4/C_1$, so Eq. (3) involves only one independent constant.

In order to simulate the seismic behavior of liquefiable deposit, the Finn built-in constitutive model was used. FLAC contains a built-in constitutive model (Finn model) that incorporates both Eqs. (2) and (3) into the standard Mohr–Coulomb plasticity model and it can be modified by the user as required.

Since there is not currently any correlation with which to obtain the calibration parameters of the model of Martin et al. [6], Byrne model [7] was used in the current paper to predict pore pressure buildup of the liquefiable soil.

For Eq. (3), Byrne [7] noted that the constant C_1 can be derived from normalized standard penetration test values, $(N_1)_{60}$,

$$C_1 = 8.7(N_1)_{60}^{-1.25}. \tag{4}$$

C_2 is then calculated from $C_2 = 0.4/C_1$ in this case.

Furthermore, using an empirical relation between D_r defined by Idriss and Boulanger [17],

$$D_r = \sqrt{(N_1)_{60}/46} \tag{5}$$

and

$$D_r = \frac{e_{max} - e}{e_{max} - e_{min}} \tag{6}$$

The values of e for each $(N_1)_{60}$ value can be calculated.

3.2. Initial condition and boundary conditions

As mentioned in Section 2, a soil mass of 32 m in height and 400 m in length was assumed for this model; the soil properties are shown in Table 1. It is assumed that sand deposit is normally consolidated (OCR = 1). This means that the soil mass before and/or after building constructions has not experienced stresses higher than its current state.

The grids located at the base of the model were fixed to the base against both horizontal and vertical movement in both static and dynamic analyses. Right and left sides of the grid were horizontally fixed for static analysis. In dynamic analyses, enough distance between the structure(s) and lateral sides should be considered to suppress the reflection of waves contacting the boundaries. Choosing adequate dimensions for the model plays an important role in modeling process. In the present work, lateral boundaries were considered as

free-field, a built-in boundary condition in FLAC for dynamic analysis. This is an alternative procedure rather than using the mentioned large distance to "enforce" the free-field motion in such a way that boundaries retain their nonreflecting properties.

Table 1. Numerical values of soil properties for the model.

Overlaid soil	Dense soil	Medium-dense soil	Loose soil	Soil condensation
30	25	15	8	$(N_1)_{60}$
0.81	0.737	0.571	0.417	D_r
19.6	19.5	18	17	γ_d (kN/m^3)
22.2	22	20.5	20	γ_{sat} (kN/m^3)
0.354	0.394	0.485	0.570	e
41.5	39.6	35.2	31.1	φ (degrees)

FLAC simulates a region of material subjected to external and/or internal dynamic loading by applying a dynamic input at either the model boundary or internal grid points. In FLAC, the dynamic input can be applied in one of the following ways: 1) an acceleration history; 2) a velocity history; 3) a stress (or pressure) history; or 4) a force history [16]. In this study, for applying earthquake loading, the acceleration time history of the Bam earthquake with magnitude M = 6.5 and maximum acceleration $a_{max} = 0.42$ g was used. Duration of the earthquake was chosen 37 s. This acceleration time history written in .ACC format is an outcrop motion and was applied to the base of the model ground.

3.3. Imported numerical quantities for the soil mass

For the soil materials, based on the state of sandy soil density we tried to define properties of materials according to weight–volume relationships.

According to the Fish function written in the FLAC program, for definition of liquefaction properties, the Byrne formula was used [7]. In this formula, according to Eq. (3), it is necessary to define two constants, C_1 and C_2. In Eq. (4), value of C_1 is related to $(N_1)_{60}$ and C_2 is related to C_1.

For determining the relative density (D_r) by $(N_1)_{60}$, the work of Idriss and Boulanger [17] (Eq. (5)) was used and assuming $e_{max} = 0.8$ and $e_{min} = 0.25$ for the sand, the quantity of e for each state of relative density according to Eq. (6) was calculated. The internal friction angle φ was also defined as follows [18]:

$$\varphi = \sqrt{15.4 \times (N_1)_{60}} + 20. \tag{7}$$

In addition to the above quantities, other parameters that are need for the model such as k_{2max} (shear modulus number), G_{max} (maximum shear modulus), and E (bulk modulus) were defined for the model by equations related to D_r (which is related to $(N_1)_{60}$ values) by a Fish function (using the relevant Seed and Idriss equations [19]). Furthermore, Poisson's ratio $\nu = 0.32$ was chosen. Table 1 summarizes the above-mentioned soil properties.

To introduce the soil condensation, parameter $(N_1)_{60}$ was used. According to Table 2, which was presented by Meyerhof [20], correlations between soil condensation and D_r are denoted. Comparison between D_r values in Table 1 and corresponding values in Table 2 shows that choosing $(N_1)_{60} = 8$, 15, and 25 for loose, medium-dense, and dense sand is correct.

Table 2. Correlations between soil condensation and D_r.

Classification	D_r (%)
Very loose	0–20
Loose	20–40
Medium	40–60
Dense	60–80
Very dense	80–100

As mentioned in Section 1, to examine the pore water pressure variation in the soil mass during the earthquake loading, the parameter r_u was defined for the software by a Fish function. Theoretically, if r_u inclines toward 1.0, effective stress inclines toward zero and liquefaction should occur. However, $r_u = 1.0$ is only the theoretical definition for liquefaction occurrence. To make a valid comparison between in situ and laboratory pore pressure responses, Hazirbaba and Rathje [21] performed a series of strain-controlled undrained cyclic simple shear tests on the same material that was used in the field experiments. Typical results from that test showed that the pore pressure generation follows a smooth progressive pattern until reaching a pore pressure ratio, r_u, of about 0.9, and the induced shear stress decreases with time and becomes extremely low as liquefaction is approached. Therefore, the lower boundary of r_u values that define liquefaction occurrence is 0.9, and if r_u reaches a value greater than 0.9 it is assumed that liquefaction happens.

3.4. Overburden

By assuming that both the building and its foundation loading are equal to 20 kPa per each m^2 for each story of the building, numerical values of extended load applied to the soil surface for each above-mentioned building are given in Table 3.

Table 3. Numerical values of applied extended loads for the model.

Number of building stories	5	10	15	20
Equivalent load (kPa)	100	200	300	400

4. Modeling results and discussion

4.1. Results of numerical modeling

4.1.1. Analyses of free-field condition

At first, for examination of model response and observation of soil mass in the free field, we tried to simulate this state with loose, medium-dense, and dense sand. In this ordinary state, without external loading, results were obtained and analyzed.

Graphic results of maximum values of r_u in the soil mass without external loading in loose, medium-dense, and dense states are shown in Figure 3.

According to the theoretical information, for loose sand with $(N_1)_{60} = 8$ (Figure 3A) and medium-dense sand with $(N_1)_{60} = 15$ (Figure 3B), due to dynamic earthquake loading, both of them were liquefied, and dense sand with $(N_1)_{60} = 25$ (Figure 3C) was not liquefied. Thus, two states of soil condensation (loose and medium-dense with $(N_1)_{60} = 8$ and 15, respectively) were chosen for numerical modeling and examination of influence of overburden on liquefaction potential.

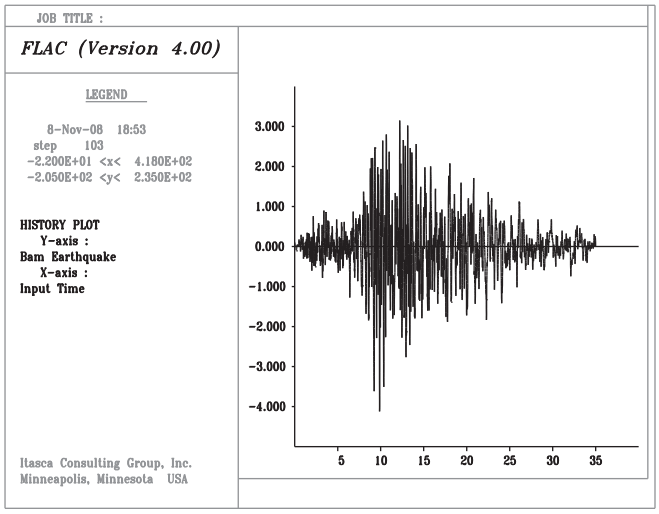

Figure 2. Acceleration time history of Bam earthquake.

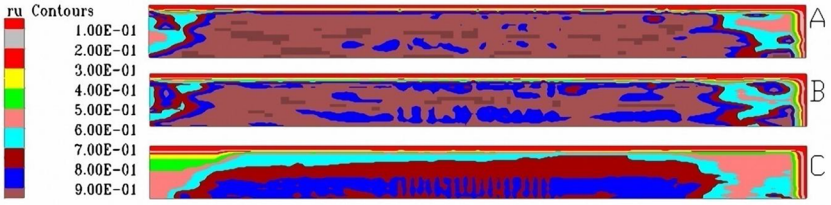

Figure 3. Maximum values of r_u in loose **(A)**, medium-dense **(B)**, and dense **(C)** sand induced by the Bam earthquake in free-field conditions (horizontal and vertical scales are different).

Figure 4 is an example of the time history of r_u during dynamic loading at a depth of 10 m in the center line of the soil mass (medium dense sand $(N_1)_{60} = 15$). It shows that the soil mass liquefied in about the 10th second of earthquake loading.

4.1.2. Static analyses

In this stage, building construction loads were applied to loose sand with $(N_1)_{60} = 8$ and medium-dense sand with $(N_1)_{60} = 15$. Figure 5 shows shear stress contours after applying static loading. The values of shear stress start to expand from two edges of buildings and the influence of shear stress becomes wider by depth. The influence of shear stress distribution under the foundation due to weight of the building and its effect on liquefaction potential will be discussed.

Figure 6, from top to bottom, shows confining effective stress contours in the case of $(N_1)_{60} = 8$ related to a 5-story building (Figure 6A), 10-story building (Figure 6B), 15-story building (Figure 6C), and 20-story building (Figure 6D), respectively. Figure 6E is related to the combined load of neighboring 10-, 15-, and 20-story buildings next to each other from right to left, respectively. According to Figures 6C–6E, applying heavy loads on the soil mass can lead to stress concentration on the edges of the loaded area and increase of initial confined effective stress in this region. This process may lead to increase in growth potential of ΔU values in the equation $r_u = \Delta U/\acute{\sigma_0}$ and, therefore, liquefaction potential in the regions near the foundation of tall buildings may increase.

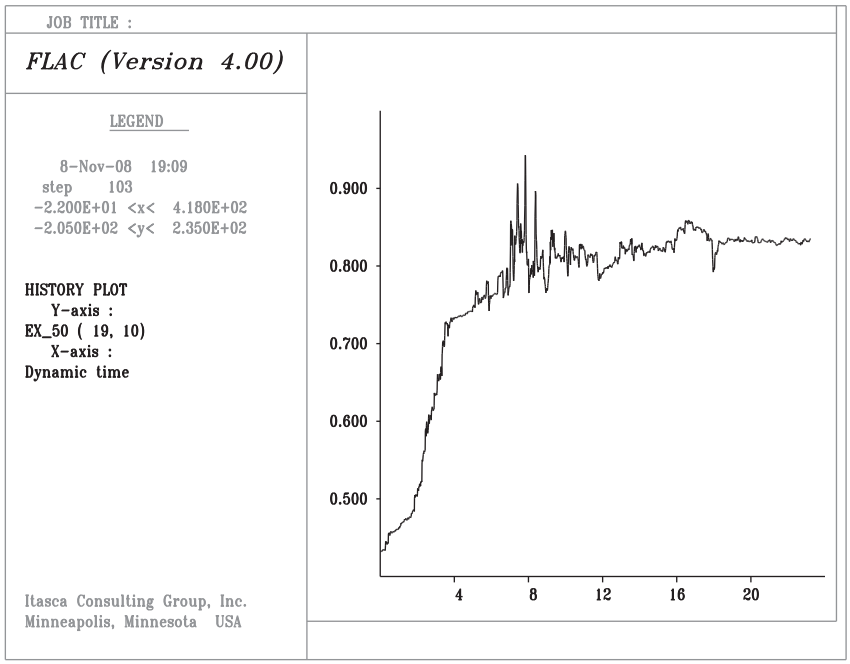

Figure 4. Time history of r_u at depth of 10 m (medium-dense sand, $(N_1)_{60} = 15$).

Figure 5. Shear stress distribution under 20-story building **(A)** and three neighboring buildings **(B)** in soil with $(N_1)_{60} = 8$.

4.1.3. Dynamic analyses

After static analyses, as a dynamic loading, acceleration time history of the Bam earthquake was applied to the model.

Maximum values of shear stains in the soil mass under loaded areas are shown in Figure 7. Comparison between states with $(N_1)_{60} = 8$ and $(N_1)_{60} = 15$ shows that maximum shear strains after dynamic loading under 5- and 10-story buildings in the case of $(N_1)_{60} = 15$ are less than corresponding values in the case of $(N_1)_{60} = 8$, but maximum shear strains under 15- and 20-story buildings are about equal. This means that tall buildings have the same effect on maximum values of shear strains induced by dynamic loading in soils with various amounts of $(N_1)_{60}$.

Figures 8A–8E and 9A–9E, from top to bottom, show maximum values of r_u related to a 5-story building (A), 10-story building (B), 15-story building (C), and 20-story building (D), respectively, while part E of these figures is related to the combined load of neighboring 10-, 15-, and 20-story buildings next to each other from right to left, respectively (refer to Figure 1).

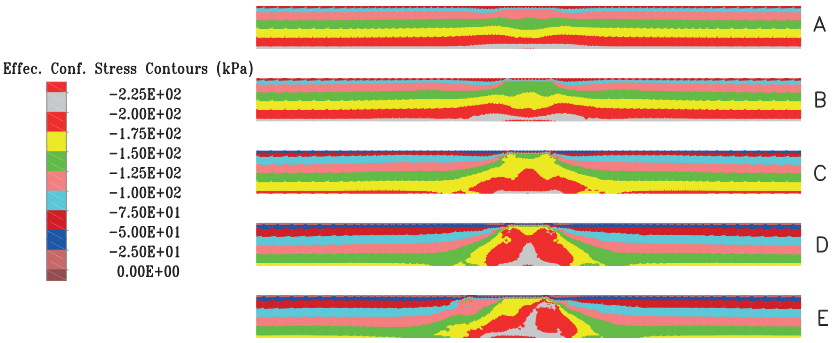

Figure 6. Confining effective stress contours in case $(N_1)_{60} = 8$ before dynamic analyses: 5-story building **(A)**, 10-story building **(B)**, 15-story building **(C)**, 20-story building **(D)**, combined load of three neighboring buildings **(E)**.

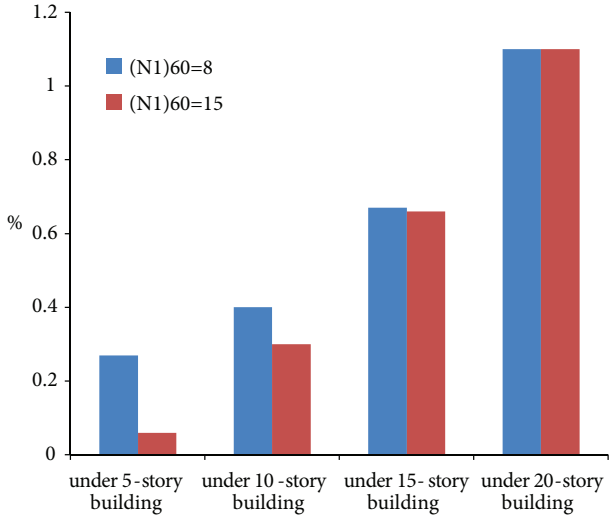

Figure 7. Maximum shear strain values in the soil mass in both $(N_1)_{60} = 8$ and $(N_1)_{60} = 15$ states after dynamic analyses.

According to Figures 8 and 9 in all cases, in general, construction loading leads to reduction in maximum values of r_u in the underlying deposits. The main reason for this is the influence of applied loading on the soil mass and increase of effective stress in the soil deposit before earthquake loading. This loading leads to an increase in both relative density and shear stress values in the soil mass. It can also be seen that by increase of external loading values, the safe area (regarding the occurrence of the liquefaction phenomenon) becomes larger. Therefore, occurrence of the liquefaction phenomenon under buildings is generally cancelled. Comparison between Figure 3 and Figures 8 and 9 shows that pore water pressure ratio distribution in the free field on each state of loading is modified by application of overburden. This result is coincident with results obtained by Lopez and Modaressi [15].

4.2. Discussion

According to Figures 8 and 9, building construction can be a reduction factor of liquefaction potential in the soil mass, but under 15- and 20-story buildings (C and D) also beneath a 20-story building (E), there is a shallow longitudinal region under the loaded area in which the maximum values of r_u reach about 0.8 to 0.9.

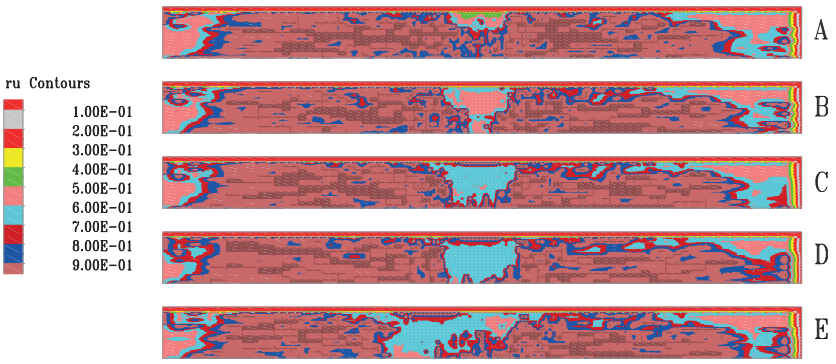

Figure 8. Maximum values of r_u in loose sand in presence of building loads induced by dynamic loading: 5-story building **(A)**, 10-story building **(B)**, 15-story building **(C)**, 20-story building **(D)**, combined load of three neighboring buildings **(E)**.

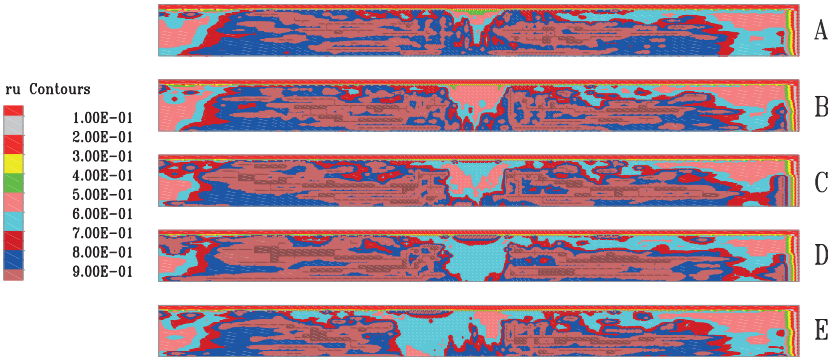

Figure 9. Maximum values of r_u in medium-dense sand in presence of building loads induced by dynamic loading: 5-story building **(A)**, 10-story building **(B)**, 15-story building **(C)**, 20-story building **(D)**, combined load of three neighboring buildings **(E)**.

In this region, the amount of effective stress increment due to external loading theoretically inclines toward the overburden value. In this case, it should be noted that a change in soil mass mechanism occurs. According to results obtained by different laboratory facilities [4], soil liquefaction strength (or CRR) decreases significantly beneath the building. The main reason for this phenomenon might be the confining pressure built up in upper layers due to heavy overburden pressure.

In the case of three buildings located next to each other, comparing the maximum values of r_u between part E and other states (B–D) in Figures 8 and 9 shows that in Figures 8E and 9E stress interactions in the soil mass due to each building probably cause a change in soil mechanism and therefore the maximum values of r_u are changed. The main reason for this change is the difference in applied stress values due to external loading on the soil mass. Thus, because of produced stress interactions under short buildings, more initial confining effective stress in comparison with previous states (Figures 8B–8D and 9B–9D) is generated (see Figure 6E). This phenomenon can be described as follows.

Due to loading on the alluvium mass, a compressive stress on loading direction under buildings is produced. This loading and compressive stress lead to compression of soil under the loaded area. Because of this action, additional stress increment on two sides of each building is established. Therefore, when several buildings are constructed beside them, the value of existent mean effective stress in the soil mass under each

building is obtained from the algebraic sum of compressive stresses in two sides of the loaded area. Increase in mean effective stress might lead to an increase in both effective confining stress and liquefaction potential in this area.

As mentioned above, the influence of shear stress distribution and effective mean stress (and/or effective confining stress) on liquefaction potential is inverse, so considering Figures 5 and 6, and also Figures 8 and 9, the increase of liquefaction potential in upper layers due to higher confining stresses is more dominant than the decrease of liquefaction potential due to shear stress distribution in this layer and, therefore, maximum values of r_u are close to 0.9 and the liquefaction probability beneath tall buildings increases. Conversely, decrease of liquefaction potential in lower layers due to shear stress distribution is more dominant than the increase of liquefaction potential due to higher confining stresses and, therefore, the probability of liquefaction occurrence in lower layers of the soil mass decreases.

From Figures 8 and 9, it can be observed that when the width of the loaded area becomes more than the thickness of the modeled ground (Figures 8E and 9E), liquefaction potential under short buildings is more than liquefaction potential under short buildings without neighbors. Pore water pressure time histories under 10- and 15-story buildings with and without neighboring buildings for the case of $(N_1)_{60} = 8$ are shown in Figures 10 and 11.

Considering Figure 2, it is obvious that maximum acceleration occurs at the 10th second. Furthermore, according to Figures 10 and 11, the maximum value of pore water pressure occurs at the 10th second. Hence, the effect of peak acceleration of earthquake loading directly affects the pore water pressure. These figures show that the maximum value of pore water pressure in the case of neighboring buildings is more than the corresponding value in the case without neighboring buildings. These figures demonstrate that as confining effective stress increases, pore water pressure variations increase. Therefore, the values of effective stress under the short buildings beside the tall buildings are less than corresponding values in the state without a neighboring building. According to Figures 6C–6E, increase of confining effective stress under short buildings due to influence of tall neighboring buildings' loading might be more than the corresponding value in the case without neighbor

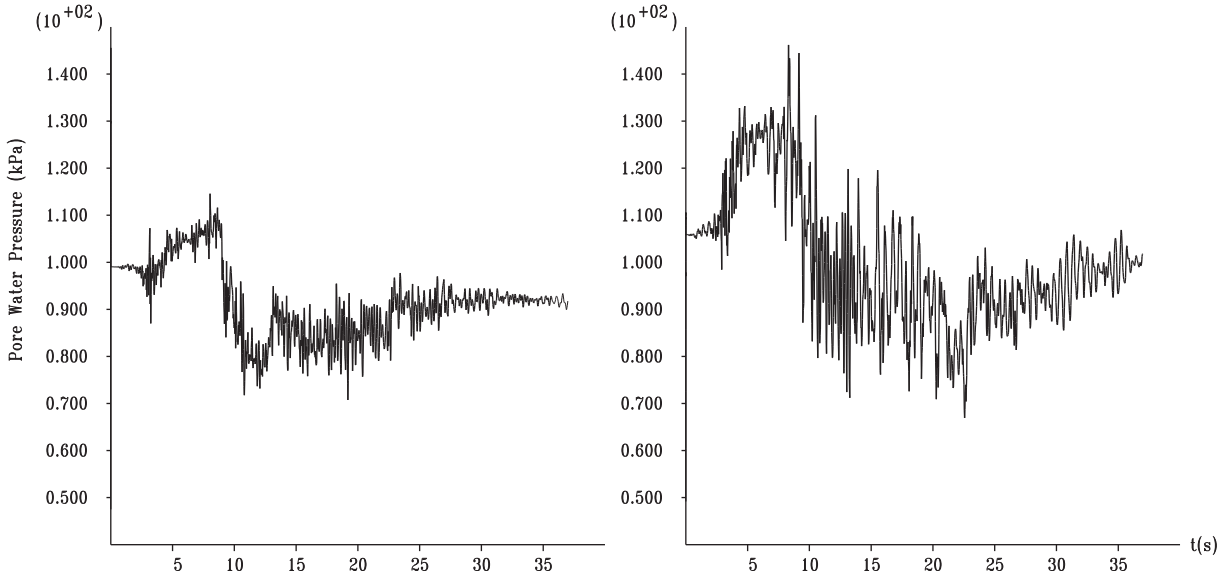

Figure 10. Time history of pore water pressure in the soil mass (depth: 10 m) located under 10-story building with neighbor building (right) and without neighbor building (left) in the case of $(N_1)_{60} = 8$.

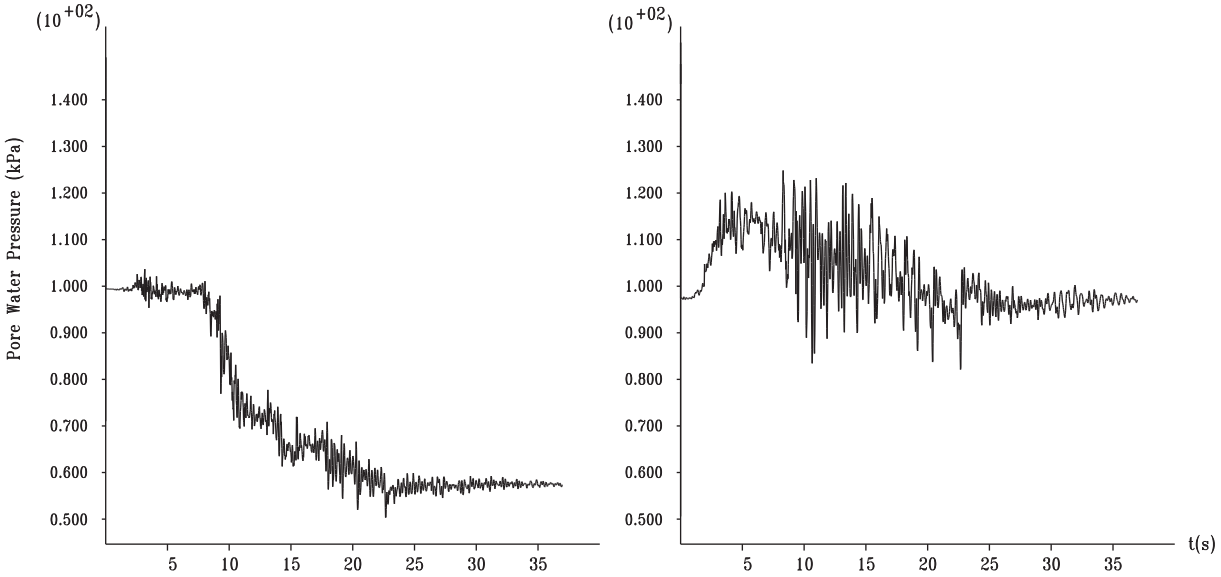

Figure 11. Time history of pore water pressure in the soil mass (depth: 10 m) located under 15-story building with neighbor building (right) and without neighbor building (left) in the case of $(N_1)_{60} = 8$.

buildings. Thus, the safe area (regarding occurrence of the liquefaction phenomenon) under a single 10-story building is larger than the corresponding area in the case with tall neighboring buildings, but this safe above-mentioned area under the 20-story building is approximately equal with corresponding area in the case with short neighboring buildings. Therefore, the influence of tall buildings on the increase of liquefaction potential of soil beneath short buildings is greater. Conversely, the short buildings have negligible effect on increase of liquefaction potential of soil beneath tall buildings.

5. Conclusions

Based on numerical results, the following conclusions can be obtained.

1. Results show that by increasing the applied loading due to building construction, the values of mean effective stress and shear stress in the soil mass increase and it generally can be a factor influencing liquefaction potential in the deposit. In general, overburden pressure leads to reduction in maximum values of r_u in the underlying deposits.

2. One of the other effective factors on the liquefaction phenomenon is generation of effective confining stress in the soil mass situated under the loaded area with high overburden pressure. Due to external loading, the value of excess effective stress in the upper layers inclines theoretically toward the applied overburden loading. The increase of effective confining stress in this region may lead to an increase in growth potential of ΔU in upper layers. The increase of ΔU in equation $r_u = \Delta U/\acute{\sigma_0}$ may lead to an increase in $r_{u\,\max}$ values and therefore the liquefaction potential in upper layers is high.

3. In the case with three buildings located next to each other, due to loading on the soil deposit, a compressive stress along the loading under loaded area is produced. This load and downward compressive stress leads to compression of soil mass under the loaded region. This action leads to an additional stress increment on two sides of the building's foundation. Therefore, when several buildings are erected beside them, the amount of existent mean effective stress in the soil mass under each building is obtained from the algebraic

sum of mean effective stresses from the above-mentioned state. In this state, pore water pressure in the soil mass is more than in the single building state. This shows that the effect of tall buildings on the increase of liquefaction potential of soil beneath short buildings is greater. Conversely, short buildings have negligible effect on the increase of liquefaction potential of soil beneath tall buildings.

4. Generally, the stress concentration and high effective confining stress in upper layers of the soil mass can be named as the factors to increase the liquefaction potential. Construction of tall buildings on the alluvium applies a heavy load to the soil and changes soil mechanisms due to stress concentration on two sides of the loaded area. Therefore, liquefaction potential in the regions near the foundation of the building increases.

References

[1] Seed HB, Idriss IM. Simplified procedure for evaluating soil liquefaction potential. Journal of the Soil Mechanics and Foundations Division 1971; 97: 1249–1273.

[2] Liyanathirana DS, Poulos HG. Numerical simulation of soil liquefaction due to earthquake loading. Journal of Soil Dynamics and Earthquake Engineering 2002; 22: 511–523.

[3] Rollins KM, Seed HB. Influence of building on potential liquefaction damage. Journal of the Soil Mechanics and Foundations Division 1990; 116: 165–185.

[4] Yoshimi Y, Tokimatsu K. Liquefaction of sand near structure during earthquake. In: Proceedings of the 4th Japan Earthquake Engineering Symposium. Tokyo, Japan; 1978. pp. 439–446.

[5] Liu H, Qiao T. Liquefaction potential of saturated sand deposits underlying foundation of structure. In: Proceedings of the 8th World Conference on Earthquake Engineering, Vol. 3. San Francisco, CA, USA; 1984. pp. 199–206.

[6] Martin GR, Finn WDL, Seed, HB. Fundamentals of liquefaction under cyclic loading. Journal of the Geotechnical Engineering Division 1975; 101: 423–438.

[7] Byrne PA. Cyclic shear-volume coupling and pore-pressure model for sand. In: Second International Conference on Recent Advances in Geotechnical Earthquake Engineering and Soil Dynamics, Vol. 1.24. St. Louis, MO, USA; 1991. pp. 47–55.

[8] Lee KL, Seed HB. Cyclic stress conditions causing liquefaction of sand. Journal of the Soil Mechanics and Foundations Division 1967; 93: 47–70.

[9] Yoshimi Y, Oh-Oka H. Influence of degree of shear stress reversal on the liquefaction potential of saturated sand. Journal of Soils and Foundations, Japanese Society of Soil Mechanics and Foundations Engineering 1975; 15: 2–40.

[10] Peacock WH, Seed HB. Sand liquefaction under cyclic loading simple shear conditions. Journal of the Soil Mechanics and Foundations Division 1968; 94: 689–708.

[11] Mulilis JP, Chan CK, Seed HB. The Effects of Method of Sample Preparation on the Cyclic Stress Strain Behavior of Sands. UCB/EERC-75/18. Berkeley, CA, USA: PEER Center; 1975.

[12] Hynes ME, Olsen R. Influence of confining stress on liquefaction resistance. In: Proceedings of International Symposium on the Physics and Mechanics of Liquefaction. Rotterdam, the Netherlands; 1998. pp. 145–152.

[13] Ishihara K, Takatsu H. Effects of over-consolidation and K_0 conditions on the liquefaction characteristics of sands. Journal of Soils and Foundations, Japanese Society of Soil Mechanics and Foundations Engineering 1979; 19: 59–68.

[14] Whitman RV, Lambe PC. Effect of boundary conditions upon centrifuge experiments using ground motion simulation. Geotech Test J 1986; 9: 61–71.

[15] Lopez CF, Modaressi FRA. Numerical simulation of liquefaction effects on seismic SSI. Journal of Soil Dynamics and Earthquake Engineering 2008; 28: 85–98.

[16] Itasca Consulting Group Inc. FLAC, Version 4.0. Minneapolis, MN, USA: Itasca Consulting Group; 2000.

[17] Idriss IM, Boulanger RW. Semi-empirical procedures for evaluating liquefaction potential during earthquakes. In: Proceedings of the 11th International Conference on Soil Dynamics & Earthquake Engineering & 3rd International Conference on Earthquake Geotechnical Engineering. Berkeley, CA, USA; 2004. pp. 32–56.

[18] Hatanaka M, Uchida A. Empirical correlation between penetration resistance and internal friction angle of sandy soils. Journal of Soils and Foundations, Japanese Society of Soil Mechanics and Foundations Engineering 1996; 36: 1–9.

[19] Seed HB, Idriss IM. Soil Moduli and Damping Factors for Dynamic Response Analyses. Report No. EERC 70-10. Berkeley, CA, USA: Earthquake Engineering Research Center, University of California; 1970.

[20] Meyerhof G. Penetration tests and bearing capacity of cohesionless soils. Journal of the Soil Mechanics and Foundations Division 1956; 82: 1–19.

[21] Hazirbaba K, Rathje EMA. Comparison between in situ and laboratory measurements of pore water pressure generation. In: 13th World Conference on Earthquake Engineering. Vancouver, Canada; 2004. Paper No. 1220.